Hic Sunt Dracones: The Structure of the Inverse-Feasible Region of a Multiobjective Integer Program

Tyler Perini[a], Daniel Qiu[b], Silviya Valeva[c], Andrew J. Schaefer[d]

[a]*Department of Mathematics, United States Naval Academy, Annapolis, MD, USA*
[b]*Department of Industrial Systems Engineering, University of Washington, Seattle, WA, USA*
[c]*Department of Decision and System Sciences, Saint Joseph's University, Philadelphia, PA, USA*
[d]*Department of Computational Applied Mathematics and Operations Research, Rice University, Houston, TX, USA*

Abstract

Optimization problems that involve multiple, conflicting criteria lead to a set of efficient solutions, and when there are discrete decisions, some solutions may be unsupported. Applications where it is difficult to estimate the parameters for criteria motivate inverse optimization techniques. We provide a theoretical analysis of the set of (unknown) objective parameters which lead to a (known) efficient subset of feasible solutions, known as the inverse-feasible region, of a multiobjective integer program. We provide insights into its structure by means of two well-structured outer approximations that help to capture its odd form. The first approximation is based on supportedness (where some solutions should be optimal for a weighted sum scalarization), and the second is based on incomparability (where no solution should dominate another). We include visualizations for the two-variable-two-objective case which help establish geometric intuition for the structure of these sets. As part of the theoretical contributions, several convexity-related subproblems are introduced, including convex cores and half-space coverings. Concluding remarks outline the remaining gaps in giving an exact representation.

Keywords: multiobjective optimization, inverse optimization, integer programs

Disclaimer: The views expressed in this article are those of the author(s) and do not reflect the official policy or position of the U.S. Naval Academy, Department of the Navy, the Department of Defense, or the U.S. Government.

1. Introduction

"Forward" optimization methods, such as linear programs (LPs) and integer programs (IPs), compute an optimal solution given an objective function and constraints when the parameter data are known *a priori*. In contexts where the parameter data are uncertain or difficult to estimate, *inverse optimization* seeks the model parameters under which a given solution (which is available *a priori*) becomes optimal. Examples of using solutions to infer parameters include: plans for intensity-modulated radiation therapy (IMRT) used to estimate model parameters (Boutilier et al., 2015; Chan et al., 2014; Hamacher and Küfer, 2002; Lee et al., 2013); seismic wave data used with inverse shortest path problems to predict movement of earthquakes (Burton and Toint, 1992a); historic behavior used to estimate difficult-to-determine costs in production planning (Troutt et al., 2006); known outcomes of an energy market used to infer a competitor's prices (Ruiz et al., 2013); and outcomes in an electricity market to recover its structure (Birge et al., 2017).

The consideration of multiple, conflicting criteria in an optimization problem is necessary for many applications across the healthcare industry (Chakraborty et al., 2023; Ehrgott et al., 2010), engineering disciplines (Andersson, 2000; Marler and Arora, 2004), and beyond (Ehrgott, 2005; Ehrgott and Gandibleux, 2002; White, 1990). Whereas the goal of single-objective optimization is to return one optimal solution, in general no "ideal" solution exists for practical applications where all objectives are optimized simultaneously. Therefore, the common goal of multiobjective optimization is to compute all *efficient solutions*, the set of which is the *efficient frontier*. Multiobjective linear programs (MOLPs) are the simplest to study since the feasible set and its image are convex polyhedra, and the efficient frontier is contained within the boundary of the feasible set polyhedron (Ehrgott, 2005).

The focus of this work is to infer objective parameters through inverse optimization for multiobjective integer linear programs (MOIPs). Prior work on inverse MOIP has focused on applications, which have developed algorithms to produce one objective matrix for a given solution or set of solutions, *e.g.*, Roland et al. (2012), Roland et al. (2013), and Roland et al. (2016). The present work aims to instead capture all such objective matrices, referred

to as the *inverse-feasible region.* Comparable analyses for inverse single-objective LPs (Ahuja and Orlin, 2001) and IPs (Schaefer, 2009) employed LP duality and superadditive duality, respectively. To date, there are only nascent concepts available for a superadditive dual of a MOIP (Dunbar et al., 2024). The present work establishes foundations for an outer description of the inverse-feasible region of a MOIP, in particular by intersecting approximations of the set using non-dual methods.

This inverse problem is fundamentally shaped by integrality. In particular, efficient solutions that are unsupported—*i.e.*, they exist in the interior of the convex hull of feasible images—arise solely due to the discrete nature of the feasible set and have no analogue in the continuous case. Unlike the case of MOLPs, convexity is not available in this discrete setting, and the unsupported solutions lead to nonconvex inverse-feasible regions. In order to compute the unsupported solutions, special techniques are required which result in convex-like properties. Our research identifies convex-adjacent subproblems, including convex cores and half-space covering.

Our main contributions can be summarized as:

- presenting novel visualization strategies to observe the structure of the inverse-feasible region of a MOIP with two variables and two objectives;
- analysis of two outer approximations of the inverse-feasible region;
- examples and structural properties of each approximation; and
- identifying open directions for future research.

Hic sunt dracones, meaning "here be dragons", is a Latin phrase used by ancient cartographers to indicate what is beyond the boundary of a current-known map; this titular phrase is appropriate for this work as it explores the boundaries of inverse optimization, multicriteria decision making, and integer programming, simultaneously. See Table 1 for a comparison of key features. We make progress into this new territory, though many aspects remain unsolved.

The outline of the manuscript is as follows. Section 2 summarizes related literature, including applications of inverse optimization. Section 3 provides preliminary definitions, and Section 4 introduces the two major outer approximations studied. Sections 5 and 6 present analyses of these approximation sets. Section 7 concludes with observations about the gap between the outer approximations and the inverse-feasible set.

Table 1: Characteristics of related problems. The counterparts of inverse, multiobjective, and discrete are forward, single-objective, and continuous, respectively.

Inverse	*Multiobjective*	*Discrete*	**Unique characteristics**
X	X		∘ Inverse-feasible region structure understood via convexity and weighted sum scalarization
X		X	∘ Inverse-feasible region structure understood via superadditive duality
	X	X	∘ Many algorithms exist for forward optimization with fixed objective matrix
X	X	X	∘ Nonconvex inverse-feasible sets have yet to be represented exactly ∘ No available duality framework ∘ Computing inverse-feasible objective matrices for unsupported efficient solutions is nontrivial

2. Literature and Applications

Among the first applications to motivate the study of (single-objective) inverse optimization were those requiring parameter estimation. Collected data (*i.e.*, observable parameters) may be used to infer the other model parameters of a physical system that are difficult or impossible to measure. In geophysics, for example, seismic wave data can be used with inverse shortest path problems to predict movement of earthquakes (Burton and Toint, 1992a); see Neumann-Denzau and Behrens (1984) and Tarantola (2005) for others. Equilibrium models are another rich area of study necessitating parameter estimation. Observed traffic data have been used to estimate congestion function parameters via inverse variational inequality problems (Bertsimas et al., 2015). Other traffic models have estimated user cost functions and traffic predictions (Burton and Toint, 1994; Zhang et al., 2016, 2018). Inverse multiobjective optimization has been motivated to compromise among a group of experts, where the nearest inverse-feasible objective matrix is sought to satisfy differing experts' evaluations (Roland et al., 2016).

Another broad area of applications for inverse optimization is the design of mechanisms within cooperative games which incentivize players to act according to the collaboratively optimal solution (Agarwal and Ergun, 2008; Houghtalen et al., 2011; Zheng et al., 2015). Building on the transportation modeling applications mentioned above, toll design problems seek to incentivize individuals to make decisions according to the network flow equilibrium, generally using cost estimations based on solving inverse optimiza-

tion problems (Dial, 1999; Marcotte et al., 2009). Applications in portfolio optimization include studies of the inverse newsvendor problem (Carr and Lovejoy, 2000), where given a set of installed capacities, the goal is to find an optimal demand distribution. In energy markets, Ruiz et al. (2013) infer a competitor's prices using known outcomes, and Birge et al. (2017) recover market structure based on observed outcomes.

The theory for inverse single-objective LPs is well established. Shortest path problems were the earliest models studied (Burton and Toint, 1992b), followed by network flow models (Ahuja and Orlin, 2001) and other combinatorial problems (Heuberger, 2004). LP duality enables an inverse LP to be formulated as a new LP (Ahuja and Orlin, 2001). Moreover, the survey by Heuberger (2004) shows that many polynomially-solvable combinatorial problems have inverse problems that are also polynomially-solvable. Some studies, like Ahuja and Orlin (2001), use a target criteria vector and seek to find the minimum perturbation from the vector that would render a given feasible solution (or set of solutions) optimal. Others focus on recovering constraints for a LP (Chan and Kaw, 2020; Ghobadi and Mahmoudzadeh, 2021). Studies of inverse optimization beyond LPs include conic and convex models (Iyengar and Kang, 2005; Keshavarz et al., 2011; Zhang and Xu, 2010; Zhang and Zhang, 2010), Markov decision processes (Erkin et al., 2010; Ghatrani and Ghate, 2023), and (mixed) integer programs (Duan and Wang, 2011; Lamperski and Schaefer, 2015; Schaefer, 2009; Wang, 2009). See Chan et al. (2023) for a recent and comprehensive review of the state of research, including applications, in single-objective inverse optimization.

This paper extends the work of Tavaslıoğlu et al. (2018), who in the context of inverse single-objective LP characterized the inverse-feasible region with respect to a (face of a) polyhedron, including dimensionality conditions. Their methodology first characterized a high-dimensional set in the space of criteria vectors and dual variables, which was then projected to the inverse-feasible region in the space of criteria vectors. Their paper illustrates inverse-feasible regions geometrically in the space of objective vectors, which was influential to this study. A common perspective for inverse optimization of MOLPs is to minimize modification of a criteria matrix (with respect to a norm) to make one feasible solution weakly efficient (Naghavi et al., 2019). Using the fact that a weakly efficient solution is optimal to the weighted sum scalarization, they establish the convex cone created by active constraints on the solution and form a nonconvex optimization problem. A series of results indicates how a set of convex optimization problems can be solved to find

the optimal criteria matrix; however, it is limited to a single feasible solution and does not provide a deeper geometric understanding of the set of inverse-feasible criteria matrices. We extend Lemma 2 of Naghavi et al. (2019) in order to achieve this understanding. Some related studies consider interior solutions and try to achieve near-efficiency (Chan et al., 2014). Our study aims to achieve efficiency for a set of feasible solutions.

We summarize three algorithmic papers for inverse MOIP and their relationship to our geometric study. First, the so-called *stability radius* of a given efficient solution is the maximal adjustment to an objective matrix (or other parameter) that maintains efficiency (Emelichev and Podkopaev, 2010; Roland et al., 2012). This work can be understood geometrically as starting with an inverse-feasible objective matrix and measuring the maximum size of a unit ball centered at that matrix which maintains feasibility (size measured by a norm, in this case, the Tchebychev norm). As our visualizations will show, the standard norms for a unit ball cannot capture the complex structure of the inverse-feasible region. Second, Roland et al. (2013) presented algorithms to compute an inverse-feasible matrix for a feasible solution and an arbitrary initial objective matrix. That is—again for a single feasible solution—how does one find the nearest inverse-feasible objective matrix to an initial infeasible one? Geometrically, this is a natural converse study, which can be understood as measuring the minimum size of a unit ball in the *complement* of the inverse-feasible set, given that the ball is centered at an infeasible point and intersects the feasible set. Lastly, Roland et al. (2016) presents algorithms for the problem when the MOIP yields a feasible ideal solution (an efficient set of cardinality one), which is motivated as compromising between multiple expert opinions for portfolio selection.

In the multiobjective literature, inverse optimization is closely related to the so-called *weight space decomposition (WSD)* methods (Alves and Costa, 2016; Helfrich et al., 2023; Köksalan and Karakaya, 2021; Przybylski et al., 2010). However, WSD is a more narrow analysis since it studies a single weighted scalarization (typically weighted sum) and assumes fixed objectives (usually three); as a result, only the few scalar weights vary. Applications which primarily optimize the weighted sum of multiple criteria, *e.g.*, IMRT treatment plan optimization (Boutilier et al., 2015; Chan et al., 2014; Lee et al., 2013), might benefit from these methods. Weighted sum scalarization is known to only capture supported solutions, whereas our analysis allows for unsupported efficient solutions.

3. Preliminaries

We begin by introducing standard definitions for multiobjective optimization before introducing notions for the inverse. For $p > 1$, let $y, z \in \mathbb{R}^p$. Isolated vectors are assumed to be column vectors, and for readability, we often omit transpose unless the dimension is not clear from context. Define the following (partial) vector orderings:

- $y < z$ if $z - y$ has all positive components;
- $y \leqq z$ if $z - y$ has all nonnegative components, where we say z *weakly dominates* y; and
- $y \leq z$ if $y \leqq z$ and $y \neq z$, where we say z *dominates* y.

Let $Y \subseteq \mathbb{R}^p$. A vector $y \in Y$ is *nondominated (ND)* with respect to Y if it is not dominated by a vector in Y. If y does not dominate z and vice versa, they are called *incomparable*, denoted by $y \sim z$. If all vectors in Y are pairwise incomparable, then Y is said to be *stable*. Note that the ND subset of any set is stable.

Consider a program with n integer decision variables, m constraints, and p objectives. We assume that constraints and objectives are defined by affine inequalities and linear functions, respectively, and henceforth we assume that the formulation is linear. For objective matrix $C \in \mathbb{R}^{p \times n}$ and $1 \leq i \leq p$, the ith row is denoted c^i and represents the vector for the ith objective. Vector $Cx \in \mathbb{R}^p$ is called the *image* of solution $x \in \mathbb{R}^n$. We consider MOIPs of the form

$$\text{MOIP}(C) \coloneqq \text{Max}\{Cx \mid Ax \leqq b, \quad x \in \mathbb{Z}^n_{\geqq}\},$$

where the "Max" operator returns the ND subset of images, the constraint matrix is $A \in \mathbb{R}^{m \times n}$, and the right-hand side vector is $b \in \mathbb{R}^m$.

The *(forward) feasible region*, $\mathcal{X} \coloneqq \{x \in \mathbb{Z}^n_{\geqq} \mid Ax \leqq b\}$, exists within the *decision space*, $\mathbb{R}^n$. Throughout this work, we assume that A and b are fixed, and that $\mathcal{X}$ is nonempty and bounded. Let $C \in \mathbb{R}^{p \times n}$ be an objective matrix, and denote the *image set* by $\mathcal{Y} \coloneqq C\mathcal{X} = \{Cx \mid x \in \mathcal{X}\}$, which exists in the *image space*, $\mathbb{R}^p$. Let $\bar{x} \in \mathcal{X}$ be a feasible solution and $\bar{y} \coloneqq C\bar{x} \in \mathcal{Y}$ be its associated image. Image $\bar{y}$ is *(weakly) nondominated (ND)* if no other feasible image $y \in \mathcal{Y}$ (strictly) dominates it; in this case, $\bar{x}$ is called a *(weakly) efficient solution*. The set of efficient solutions is called the *efficient frontier*, denoted $\mathcal{X}_E(C)$, and the set of ND images is called the *ND frontier*.

In the analysis of the ND set of a MOIP, the concept of the convex hull is critical to classifying solutions and images. A *scalarization* replaces a vector-valued objective function with a scalar-valued objective function. The most common scalarization, called the *weighted sum scalarization*, uses a weight vector $\lambda \in \mathbb{R}^p$ and is defined as:

$$\max\{\lambda^\top Cx \mid x \in \mathcal{X}\}. \tag{1}$$

If x^* is optimal for (1) with $\lambda \in \mathbb{R}^p_>$ ($\mathbb{R}^p_\geq$), then x^* is (weakly) efficient. Moreover, its image lies on the (weakly) ND boundary of $\text{conv}(\mathcal{Y})$. Hence, for $x^* \in \mathcal{X}_E(C)$, if there exists $\lambda \in \mathbb{R}^p_\geq$ such that x^* is optimal to the weighted sum scalarization, then the solution and its image are said to be *supported*. When an efficient solution cannot be optimal to weighted sum scalarization, as can only be seen in the discrete setting, the solution and its image are called *unsupported*. Let $\mathcal{X}_{SE}(C)$ denote the set of supported efficient solutions to MOIP(C). The relationship between convexity and this scalarization illustrates why analysis by this scalarization faces the same limitations as convex analysis. The challenge arises with the search for unsupported ND images that lie in the interior of $\text{conv}(\mathcal{Y})$; this is especially important when the ratio of unsupported images in a ND set is nontrivial.

The (typical) *forward* MOIP is to solve for the efficient frontier given complete information, *i.e.*, fixed A, b, and C. However, the *inverse* problem we analyze here is: given A, b, and a target subset of feasible solutions, determine an explicit description for the set of objective matrices such that the target subset coincides with the efficient frontier. For instance, let $x^0 \in \mathcal{X}$. We say an objective matrix $C \in \mathbb{R}^{p\times n}$ is *inverse-feasible for solution* x^0 if $x^0 \in \mathcal{X}_E(C)$. More generally, we consider a set of solutions $\bar{X} \coloneqq \{x^1, \ldots, x^s\} \subseteq \mathcal{X}$, where $s \geq 1$.

Definition 1. *An objective matrix $C \in \mathbb{R}^{p\times n}$ is said to be* inverse-feasible *for set $\bar{X}$ if $\bar{X} = \mathcal{X}_E(C)$. We define the* inverse-feasible region *as the set of objective matrices such that $\bar{X}$ is the efficient frontier of MOIP(C), denoted by*

$$D^*_E(\bar{X}) \coloneqq \{C \in \mathbb{R}^{p\times n} \mid \bar{X} = \mathcal{X}_E(C)\}.$$

A more strict representation of the inverse-feasible region, which will be more amenable to our analysis, is additionally conditioned on the target supported solutions, $\bar{X}_{SE} \subseteq \bar{X}$:

$$D^*_E(\bar{X}, \bar{X}_{SE}) \coloneqq \{C \in \mathbb{R}^{p\times n} \mid \bar{X} = \mathcal{X}_E(C) \text{ and } \bar{X}_{SE} = \mathcal{X}_{SE}(C)\}.$$

We introduce new labels for the space of (multi)objective matrices, $\mathbb{R}^{p\times n}$, as the *inverse-matrix space*, and the space of (single-)objective vectors, $\mathbb{R}^n$, as the *inverse-vector space*. While inverse-vector space coincides in dimension with decision space, they intuitively relate to very different concepts, and so the distinct labels will facilitate our presentation.

3.1. Inverse-Feasible Regions for Single-Objective IPs

Consider analyzing a single-objective IP (fixed $p = 1$). We denote the objective vector by $c \in \mathbb{R}^n$, and the (scalar) optimal value by

$$\mathrm{IP}(c) \coloneqq \max\{cx \mid Ax \leqq b, \quad x \in \mathbb{Z}^n_{\geqq}\}.$$

Two continuous relaxations of this discrete problem are important. First, the LP relaxation removes integrality constraints (replaces $x \in \mathbb{Z}^n_{\geqq}$ with $x \in \mathbb{R}^n_{\geqq}$), which in general does not yield a tight relaxation. Second, the convex hull relaxation replaces the constraint set with $x \in \mathrm{conv}\{Ax \leqq b \mid x \in \mathbb{Z}^n_{\geqq}\}$ and is the tightest possible relaxation for single-objective IPs.

Definition 2. *Let $\bar{x} \in \mathcal{X}$. The inverse-feasible region for the single-objective problem is denoted by*

$$D^*(\bar{x}) = \{c \in \mathbb{R}^n \mid c\bar{x} = IP(c)\}.$$

Note that the notation is without subscript and with a single solution as input. For any $\bar{x} \in \mathcal{X}$, $D^*(\bar{x})$ is always a polyhedral, pointed cone, including the case that $D^*(\bar{x}) = \{\vec{0}\}$.

Remark 1. *The role of integrality is crucial to distinguishing this work from that of inverse MOLPs. First, integrality of $\mathcal{X}$ means that the D^* cones are dependent upon the ideal formulation for* $\mathrm{conv}(\mathcal{X})$*; in the simpler LP case, the constraints inscribing $\mathcal{X}$ are sufficient. Second, an efficient solution may only be unsupported in the discrete case. All the complex phenomena of this paper—nonconvexity and gaps between approximation sets—disappear in the continuous case.*

The boundaries of the $D^*(x)$ cones relate to the isoprofit objective vectors, which are central to our study.

Definition 3. *Nonzero $c^* \in \mathbb{R}^n$ is an* isoprofit objective vector *for $x^1, x^2 \in \mathcal{X} \subset \mathbb{R}^n$ if x^1 and x^2 are simultaneously optimal solutions to IP(c^*). As the name suggests, an isoprofit objective vector equally values two given solutions, and there exists $d \in \mathbb{R}$ such that $c^*x^1 = c^*x^2 = d$.*

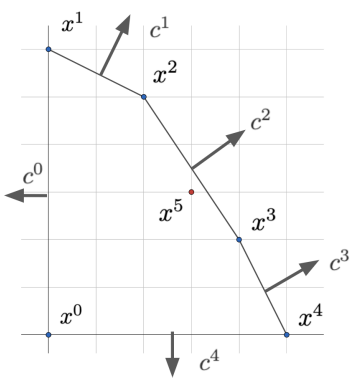

(a) Forward feasible set illustrated in decision space.

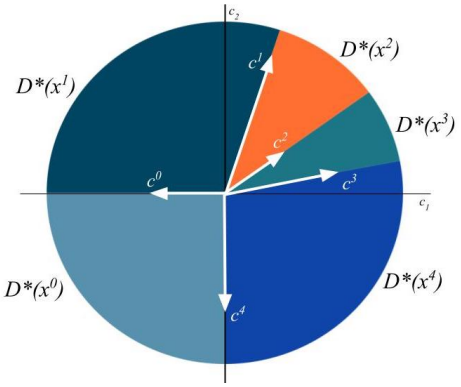

(b) Single-objective inverse-feasible sets illustrated in inverse-vector space.

Figure 1: Example 1.0 with isoprofit objective vectors.

3.2. Running Examples and Visualizations

The following running example is used to demonstrate concepts throughout the manuscript, beginning with the single-objective definitions introduced thus far.

Example 1.0. *Let a discrete (forward) feasible set $\mathcal{X} \subset \mathbb{Z}^2$ be defined by the following linear constraints:*

$$\mathcal{X} := \{x \in \mathbb{Z}^2_{\geqq} \mid x_1 + 2x_2 \leq 12, \quad 3x_1 + 2x_2 \leq 16, \quad 2x_1 + x_2 \leq 10\}.$$

See Figure 1a. The extreme points of the convex hull are labeled as: $x^0 = (0,0)$, $x^1 = (0,6)$, $x^2 = (2,5)$, $x^3 = (4,2)$, and $x^4 = (5,0)$. Isoprofit objective vectors for adjacent extreme points are as follows: $c^0 = [-1,0]$, $c^1 = [1,2]$, $c^2 = [3,2]$, $c^3 = [2,1]$, and $c^4 = [0,-1]$. Solution $x^5 = (3,3)$ is noteworthy to distinguish between single-objective optimality and multiobjective efficiency: As it is not on the boundary of $\text{conv}(\mathcal{X})$*, it is not optimal for any single objective including weighted sum scalarization. However, it still may be (unsupported) efficient for certain objectives (see Example 1.2).*

We use Example 1.0 to demonstrate the three visual representations recurring throughout the manuscript.

Decision space. Figure 1a is a traditional visualization technique representing the (forward) feasible set, $\mathcal{X}$, in decision space, $\mathbb{R}^2$.

Inverse-vector space. Figure 1b is a second visualization technique that represents inverse-feasible objective vectors in inverse-vector space (also $\mathbb{R}^2$), where individual objectives can be shown. For simplicity, we choose to depict the inverse-feasible region as restricted to the unit disk, *i.e.*, vectors have a maximum Euclidean length of one.

Example 1.1. *In Figure 1b, the cones emanating from the origin, labeled by $D^*(x^i)$, denote the set of objective vectors for which x^i is optimal for the single-objective IP. In fact, the rays defined by isoprofit vectors c^0, c^1, c^2, c^3, and c^4 form the* boundaries *of the inverse-feasible sets $D^*(x^0), \ldots, D^*(x^4)$. Note that $D^*(x^5) = \{\vec{0}\}$ (not labeled) since it is only optimal for the zero objective vector.*

Visualization of decision space and inverse-vector space is limited to $n \leq 3$, but for demonstration purposes, we only include an example for $n = 2$. The inverse-vector space is useful for visualizing just one objective matrix comprised of multiple objective vectors, but it becomes limited when trying to visualize multiple objective matrices. Since the inverse-feasible region will contain many matrices, this visualization is inadequate, which motivated the following tool to overcome this challenge.

θ-space. For the particular case of two variables and two objectives ($n = p = 2$) and objective matrices with nonzero rows, we may use polar coordinate representation of each objective vector to achieve a 2-dimensional representation of all objective matrices. For a nonzero objective vector $c^i \in \mathbb{R}^2$ represented as (r^i, θ^i), the magnitude r^i is immaterial and therefore omitted; only the angle θ^i matters. (The nonuniqueness of θ^i is addressed later.) Hence, this visualization technique, which we call *θ-space*, uses $\mathbb{R}^2$ to illustrate the (θ^i, θ^j) pairs representing the objective vectors for a set of biobjective matrices of the form $C = [c^i; c^j]$.

Remark 2. *It is possible to use spherical coordinates to represent the case of three variables, but this would suffer from the challenges of a 3-dimensional visualization. We only recommend this technique for two variables.*

Remark 3. *For a zero objective vector, every feasible solution is optimal. A solution in the interior of* $\text{conv}(\mathcal{X})$ *is only optimal for the zero objective vector. As a result, there are no empty D^* cones. We exclude cases where all feasible solutions are efficient, so zero objective vectors are excluded from our claims. The polar representation of zero vectors are undefined.*

Example 1.2. *Consider the running example as a biobjective IP with the identity objective matrix:*

$$\text{Max} \left\{ \begin{pmatrix} 1 & 0 \\ 0 & 1 \end{pmatrix} x \mid x \in \mathcal{X} \right\}.$$

Note that the solution set, $\mathcal{X}$, is equivalent to the image set, $\mathcal{Y}$, and that x^5 is an efficient solution (ND image) here because no other integer feasible solution (image) dominates it. Therefore, the efficient set is $\mathcal{X}_E = \{x^1, x^2, x^3, x^4, x^5\}$. Denote the objective vectors by $c^1 = (1, 0)$ and $c^2 = (0, 1)$, whose polar representations are $(1, 0)$ and $(1, \frac{\pi}{2})$, respectively. Therefore, the identity objective matrix $C = [c^1; c^2]$ is represented by coordinate pair $(\theta^1, \theta^2) = (0, \frac{\pi}{2})$. Similarly, the permuted objective matrix $C = [c^2; c^1]$ is represented by coordinate pair $(\theta^2, \theta^1) = (\frac{\pi}{2}, 0)$. Each matrix is represented as a single point in Figure 2a, and note the symmetry across the $\theta_2 = \theta_1$ line.

The objective vectors from Example 1.0 have the following polar representations, (r^i, θ^i): $(1, \pi)$, $(\sqrt{5}, \arctan 2)$, $(\sqrt{13}, \arctan \frac{2}{3})$, $(\sqrt{5}, \arctan \frac{1}{2})$, and $(1, \frac{3\pi}{2})$. Hereon the radii are omitted. Recall that a (nonzero) vector with polar angle θ is also equivalently represented by $\theta \pm 2\pi k$ for all $k \in \mathbb{Z}$. In our θ-space visualizations, this is observable as a continuation across the right-most edge and the left-most edge of the graph, and continuation across the top-most edge and the bottom-most edge (in "Pacman"-like fashion, see Figure 2b).

Figure 2b is a stylistic representation of our research questions for the inverse MOIP problem: What other objective matrices lead to the same efficient frontier? What are the shape and size of the inverse-feasible regions? As a preview, Figures 2c and 2d demonstrate some of the inverse-feasible regions for Example 1.0 computed by brute force grid search. First, Figure 2c shows the inverse-feasible regions when $\bar{X}$ is a singleton, *i.e.*, $D_E^*(\{x^i\})$. In θ-space, each of these regions appears as a convex square along the diagonal. (The singleton case is the bridge between the single-objective perspective and our new multiobjective understanding.) Second, Figure 2d shows the more complex inverse-feasible regions when $\bar{X}$ contains a second solution. Appendix A displays the remaining inverse-feasible regions. Section 4 characterizes these structures by intersecting approximations.

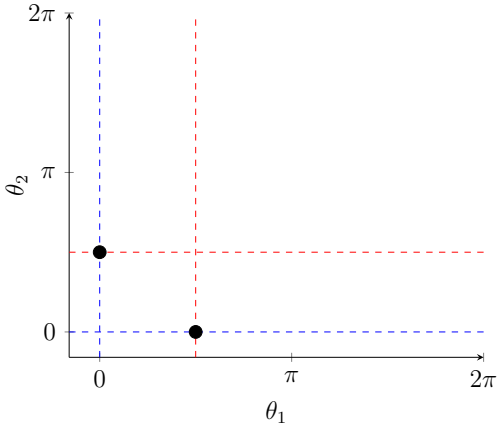

(a) θ-space representations of objective matrices $[1, 0; 0, 1]$ and $[0, 1; 1, 0]$.

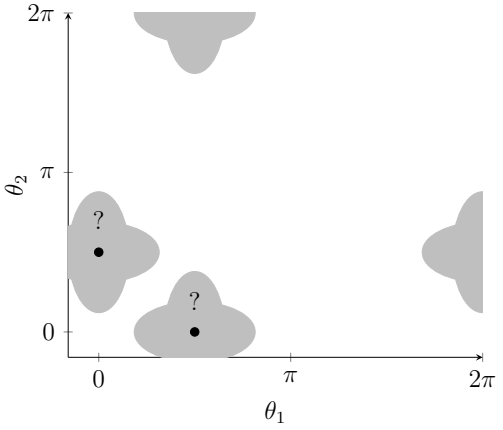

(b) The inverse optimization problem asks: what is the *shape and size* of the inverse-feasible set, illustrated in gray?

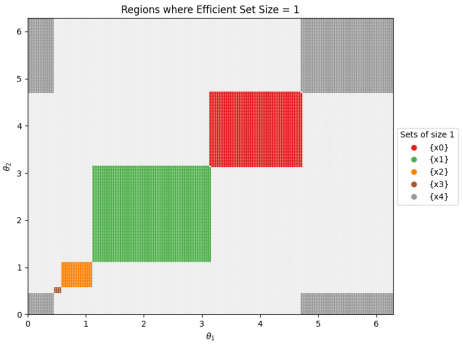

(c) Inverse-feasible sets (distinguished by color) when the efficient set is a singleton.

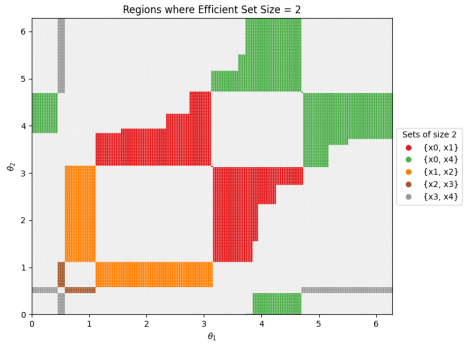

(d) Inverse-feasible sets (distinguished by color) for efficient sets comprised of two solutions.

Figure 2: Illustrating the biobjective inverse optimization problem in θ-space. Note that θ-space visuals continue from the right edge to the left edge (and from the bottom edge to the top edge) due to the periodicity of polar angles.

4. Outer Approximations for the Inverse-Feasible Region

Recall that $\bar{X} \subset \mathcal{X}$ is a given target set of solutions that should be efficient, and our aim is to approximate the inverse-feasible region, $D_E^*(\bar{X})$. Two relaxations for $D_E^*(\bar{X})$ are presented which are understood to be nontight but are amenable to analysis. The first outer approximation is referred to as the *inverse supported set*, which is only conditioned on a target subset that should be supported, denoted $\bar{X}_{SE} \subseteq \bar{X}$. The inverse supported set is

defined as

$$D^*_{SE}(\bar{X}_{SE}) \coloneqq \{C \in \mathbb{R}^{p\times n} \mid \bar{X}_{SE} = \mathcal{X}_{SE}(C)\}, \tag{2}$$

which is analogous to D^*_E except that $\mathcal{X}_E(C)$ is replaced by the supported counterpart $\mathcal{X}_{SE}(C)$. Importantly, set D^*_{SE} will always be simpler to analyze since a supported efficient solution is optimal to a single-objective problem, and hence we may rely on analytical tools from single-objective optimization. The second outer approximation, referred to as the *inverse incomparable set*, is defined as

$$\tilde{D}(\bar{X}) \coloneqq \{C \in \mathbb{R}^{p\times n} \mid C\bar{X} \text{ is stable}\}. \tag{3}$$

This second approximation allows to incorporate features of the efficient set that are unique to MOIPs, in particular, the existence of unsupported efficient solutions. Sections 5 and 6 analyze these approximations, respectively.

Property 1 and Figure 3 summarize the subset relationship between the sets. What follows is more in-depth discussion of the more nuanced relationships between these approximations.

Property 1. *Let $\bar{X} \subseteq \mathcal{X}$ such that $D^*_E(\bar{X})$ is nonempty. For some $C \in D^*_E(\bar{X})$, let $\bar{X}_{SE} = \mathcal{X}^*_{SE}(C)$. Then*

$$D^*_E(\bar{X}, \bar{X}_{SE}) \subseteq D^*_{SE}(\bar{X}_{SE}) \cap \tilde{D}(\bar{X}).$$

Proof. Suppose that $C \in D^*_E(\bar{X})$, and let $\mathcal{Y} = C\mathcal{X}$. Then every image in $C\bar{X}$ is ND with respect to $\mathcal{Y}$, which implies image set $C\bar{X}$ is stable. Thus, $C \in \tilde{D}(\bar{X})$. By assumption, there exists C such that $C\bar{X}_{SE}$ is the supported efficient subset of $\mathcal{Y}$. Since $C \in D^*_E(\bar{X})$ and $\bar{X}_{SE} = \mathcal{X}^*_{SE}(C)$, we trivially have $C \in D^*_{SE}(\bar{X}_{SE})$. □

Consider the following observations about the assumptions of Property 1. The given target set is $\bar{X}$, from which we assume the inverse problem is feasible and choose one inverse-feasible objective matrix, C, to act as the "ground truth." Set $\bar{X}_{SE}$ is the supported efficient set for this ground truth objective matrix. It is understood that the supported subset depends on the choice of C; however, this nuance is inconsequential to this study since we expect that $\bar{X}_{SE}$ will be given. Said another way, there is no uniqueness claim made in Property 1. For instance, given $\bar{X}$, neither C is the unique objective matrix for which $\bar{X}$ is the efficient set, nor $\bar{X}_{SE}$ is the unique supported set when $\bar{X}$ is efficient. In doing so, the property generalizes appropriately to all inverse-feasible matrices, C. Additionally, when all efficient solutions are supported ($\bar{X}_{SE} = \bar{X}$), the following two sets coincide: $D^*_E(\bar{X}) = D^*_{SE}(\bar{X})$.

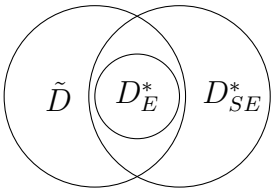

(a) The relationship between target set $D_E^*(\bar{X}_E)$ and outer approximations $\tilde{D}(\bar{X})$ and $D_{SE}^*(\bar{X}_{SE})$ for fixed sets $\bar{X}_{SE} \subseteq \bar{X}_E \subseteq \bar{X}$.

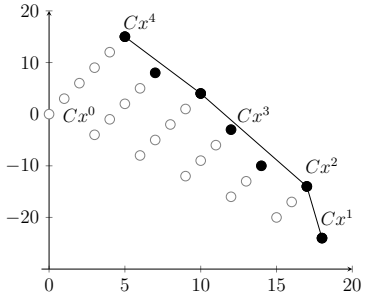

(b) The image set for biobjective matrix $C = [1, 3; 3, -4]$. Here, $C \in \tilde{D}(\bar{X}_E) \setminus D_{SE}^*(\bar{X}_E)$ since all target solutions are mutually incomparable, however the supported solutions do not match the target set $\bar{X}_{SE}$.

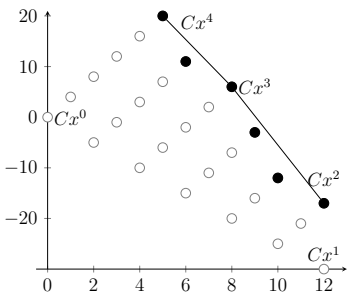

(c) The image set for biobjective matrix $C = [1, 2; 4, -5]$. Here, $C \in D_{SE}^*(\bar{X}_{SE}) \setminus \tilde{D}(\bar{X}_E)$ since all target solutions are supported, however x^1 is dominated, so $\bar{X}_E$ is not stable.

Figure 3: Representations of the outer approximation sets, including objective matrices not contained in D_E^*. For (b) and (c), the solution set is given in Example 1.0, the target efficient set is $\bar{X}_E = \{x^1, x^2, x^3, x^4\}$, and the target supported set $\bar{X}_{SE} = \{x^2, x^3, x^4\}$. ND images are darkened, and the supported images are outlined.

Note that there is not a generalizable containment relationship between the sets $D_{SE}^*(\bar{X}_{SE})$ and $\tilde{D}(\bar{X})$ (in either direction); there are typically overlapping and disjoint portions, as demonstrated by Figures 3(b) and (c). Assume $\bar{X}_{SE} \subset \bar{X}_E \subset \bar{X}$. It may often be the case that there exists $C \in D_{SE}^*(\bar{X}_{SE}) \setminus \tilde{D}(\bar{X})$, which yields a dominated image in $C\bar{X} \setminus C\bar{X}_{SE}$. Similarly, there may often exist $C' \in \tilde{D}(\bar{X}) \setminus D_{SE}^*(\bar{X}_{SE})$, which yields a stable ND set but not the appropriate (un)supported images.

Example 1.3. *From the running example, let* $\bar{X} = \bar{X}_{SE} = \{x^1, x^2\} = \{(0, 6), (2, 5)\}$. *Figure 4 illustrates the important sets we study. Observe both subset relationships* $D_E^*(\bar{X}) \subseteq D_{SE}^*(\bar{X}_{SE})$ *and* $D_E^*(\bar{X}) \subseteq \tilde{D}(\bar{X})$. *For this instance, we coincidentally have that* $D_{SE}^*(\bar{X}_{SE}) \subset \tilde{D}(\bar{X})$, *and so one approximation is tighter. (This does not generalize.)*

The following subsections address matrices of special structure and what role they play (or do not play) in our analysis.

4.1. Symmetry by Permutation

The definitions of dominance and incomparability are *symmetric under permutation* of objective indices. For instance, when image set $C\bar{X}$ is stable

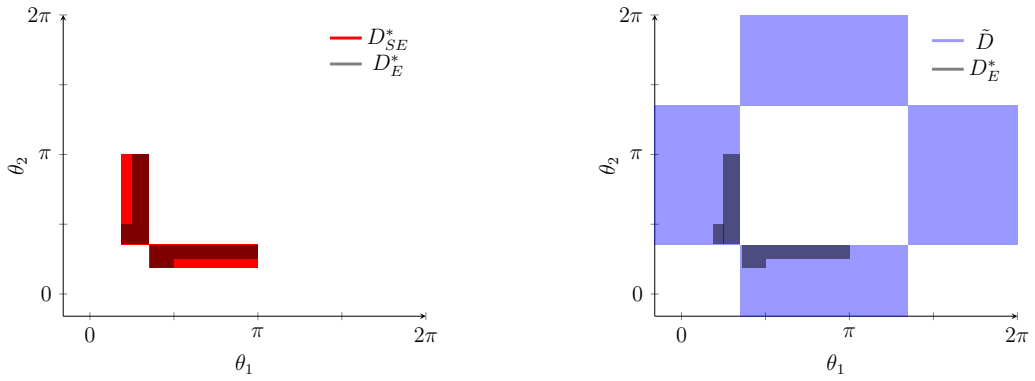

Figure 4: The target inverse-feasible set, $D^*(\bar{X})$, is illustrated in θ-space, superimposed, as two dark gray, L-shaped regions. The outer approximation based on supportedness, $D^*_{SE}(\bar{X}_{SE})$, are two boxes in red. The outer approximation based on stability, $\tilde{D}(\bar{X})$ is illustrated in blue as a union of boxes.

for objective matrix $C = [c^1; \ldots; c^p]$, then the image set will remain stable for any permutation (relabeling) of these objectives. Hence, Property 2 states that the sets D^*_E, D^*_{SE}, and $\tilde{D}$ are all closed under permutation.

Property 2. *Let $\emptyset \subset \bar{X}_{SE} \subseteq \bar{X} \subseteq \mathcal{X}$ and $c^1, \ldots, c^p \in \mathbb{R}^n$. Objective matrix $[c^1; \ldots; c^p] \in D^*_E(\bar{X}, \bar{X}_{SE})$ if and only if $[c^{\sigma(1)}, \ldots, c^{\sigma(p)}] \in D^*_E(\bar{X}, \bar{X}_{SE})$ for all permutations $\sigma : \{1, \ldots, p\} \to \{1, \ldots, p\}$. The same is true for $D^*_{SE}(\bar{X}_{SE})$ and $\tilde{D}(\bar{X})$.*

Symmetry facilitates computation because certifying one element does (not) belong to a set implies certification of more elements by permutation. The symmetry of Property 2 can be observed in θ-space visuals as symmetry over the line $\theta_2 = \theta_1$.

4.2. Trivial Objective Matrices

In the multiobjective setting, the zero objective matrix maps every feasible solution to the origin, so trivially the image set is stable, and all feasible solutions are efficient and supported.

Property 3. *For any $\emptyset \subset \bar{X} \subseteq \mathcal{X}$, the zero objective matrix is feasible to the inverse incomparable set, i.e., $\mathbf{0} \in \tilde{D}(\bar{X})$. The zero objective matrix is inverse-feasible, i.e., $\mathbf{0} \in D^*_E(\bar{X}, \bar{X}_{SE})$, if and only if $\bar{X}_{SE} = \bar{X} = \mathcal{X}$.*

By Property 3, the MOIP inverse-feasible region may be empty, which is unlike the single-objective case. This is in part due to the strictness of the definition of $D^*_E(\bar{X}, \bar{X}_{SE})$.

4.3. Self-Conflicting Objective Matrices

A broader class of objective matrices is always feasible to the inverse incomparable set, $\tilde{D}(\bar{X})$.

Definition 4. *We say objectives* c^1 *and* c^2 perfectly conflict *(or are* perfectly conflicting*) if* $c^2 = -\alpha c^1$ *for some scalar* $\alpha > 0$*. An objective matrix* C *is said to be* self-collinear *if for every row* $j > 1$ *there exists nonzero* α^j *such that* $c^j = \alpha^j c^1$ *with at least one negative* α^j*.*

This property is stronger than having row rank of one. For example, let $c \in \mathbb{R}^n$ be nonzero and fixed. Then $C = [c; 2c; 3c; 4c]$ is not self-collinear by our definition (even though every row vector belongs to one line), but $C' = [c; -2c; 3c; 4c]$ satisfies our definition due to the negative second row. Self-collinear objective matrices are not inherently practical or insightful for most applications. However, Property 4 shows that they are always feasible to the outer approximation $\tilde{D}$. We include a proof for the biobjective case which generalizes to $p > 2$.

Property 4. *For any* $\bar{X} \subseteq \mathcal{X}$ *and self-collinear objective matrix* C*,* $C\bar{X}$ *is stable.*

Proof. The cases $|\bar{X}| = 0$ and $|\bar{X}| = 1$ are trivial. We prove the claim for $|\bar{X}| > 1$ and $p = 2$. Let the self-collinear objective matrix be $C = [c^1, -\alpha c^1]$ for $\alpha > 0$, and let x^1, $x^2 \in \bar{X}$ be distinct. We denote the associated images as $y^1 = (c^1x^1, -\alpha c^1x^1)$ and $y^2 = (c^1x^2, -\alpha c^1x^2)$. We have 3 cases: (i) If $c^1x^1 = c^1x^2$, then the second components also coincide, $-\alpha c^1x^1 = -\alpha c^1x^2$, and therefore $y^1 = y^2$ and so $y^1 \sim y^2$. (ii) If $c^1x^1 < c^1x^2$, then $-\alpha c^1x^1 > -\alpha c^1x^2$. They are again incomparable. The remaining case (iii) follows from the reverse argument for (ii). Since x^1 and x^2 are chosen arbitrarily, we can conclude that all elements of $\bar{X}$ are pair-wise incomparable, and hence it is a stable set. Furthermore, the image set belongs to a line, *i.e.*, $C\bar{X} \subset \{y \in \mathbb{R}^2 | y_2 = -\alpha y_1\}$, such that every image is efficient and supported. These arguments generalize to $p > 2$. □

5. Properties of Inverse Supported Set

We have defined the inverse-feasible set, $D_E^*(\bar{X}, \bar{X}_{SE})$, as a function of two input sets: $\bar{X}$ is the target set of efficient solutions and $\bar{X}_{SE}$ is the target set of supported solutions. In the special case that $\bar{X}_{SE} = \bar{X}$ (*i.e.*, there

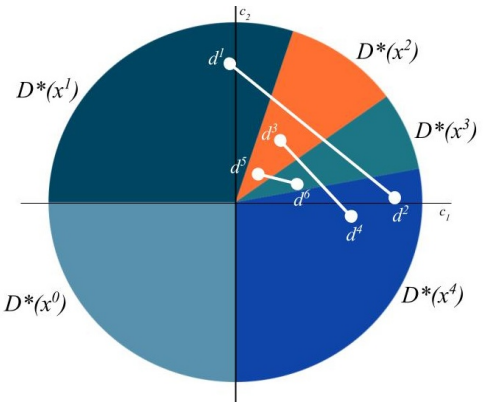

Figure 5: Inverse-vector space for Example 1.0. Objective vectors are illustrated by points. For a biobjective matrix with two objective vectors, the line segment indicates the objectives possible via weighted sum scalarization.

are no unsupported solutions as is the case in MOLP), then we have that $D_E^*(\bar{X}_{SE}, \bar{X}_{SE})$ reduces equivalently to the inverse supported set $D_{SE}^*(\bar{X}_{SE})$. This special case can be almost entirely understood through means of single-objective methods, in particular, weighted sum scalarization. This natural starting point was leveraged for MOLPs by Naghavi et al. (2019). However, it is most practical to assume that $\emptyset \subset \bar{X}_{SE} \subset \bar{X} \subset \mathcal{X}$, with all subsets being strict. We develop geometric intuition for the inverse supported set in an incremental way.

Consider the biobjective case with two variables ($n = p = 2$). Suppose an objective matrix $D \in \mathbb{R}^{2\times 2}$ is inverse-feasible. Then both objectives d^1 and d^2 can be illustrated in inverse-vector space as individual points. The challenge for visualization becomes how to indicate that these two points should be treated as a single matrix. In Figure 5, we choose to link the two points by a line segment. For instance, $D = [d^1; d^2]$ is the first objective matrix, $D' = [d^3; d^4]$ is a second, and $D'' = [d^5; d^6]$ is a third. This strategy is only sufficient for visualizing a few objective matrices, since the figure becomes increasingly dense as the number of matrices increases.

This visualization provides an additional interpretation: For $D = [d^1; d^2]$, the line segment linking d^1 and d^2 is the set of convex combinations of these two objective vectors. Hence, it equivalently represents all possible weighted sum scalarization objectives (with respect to d^1, d^2, and nonnegative weights that sum to one). We can use this intuition to identify which solutions are then supported for a fixed pair of objectives: every cone $D^*(x^i)$ intersected

by the line segment is a supported solution in the efficient frontier.

Example 1.4. *Let $D = [d^1; d^2]$. The line segment in Figure 5 depicts the convex hull,* $\text{conv}\{d^1, d^2\}$*, and has nonempty intersection with $D^*(x^i)$ for $i = 1, 2, 3, 4$. Hence, for objective matrix D, $X_{SE} = \{x^1, x^2, x^3, x^4\}$. Similarly, for objective matrix $D' = [d^3; d^4]$, $X_{SE} = \{x^2, x^3, x^4\}$. Finally, for objective matrix $D'' = [d^5; d^6]$, $X_{SE} = \{x^2, x^3\}$.* □

In the same way, an objective matrix for $p \geq 3$ could be represented by the convex hull of p objective vectors. The following result states the general equivalence between convex combinations of objective vectors and the inverse feasibility of D^*_{SE}. The key link is that supportedness is defined by the weighted sum scalarization, and the convex hull in inverse vector space captures all possible nonnegative weights. The following extends Lemma 2 (Naghavi et al., 2019) from the case of MOLPs and one solution to the case of MOIPs and a set of solutions. Excluded proofs are in the Supplementary Materials.

Lemma 1. *Let $\mathcal{X}$ and $C := [c^1; \ldots; c^p]$ be given such that $c^1, \ldots, c^p \in \mathbb{R}^n$ are nonzero and C is not self-collinear. The supported efficient set $X_{SE}(C)$ is the collection of solutions whose D^* cone intersects the interior of* $\text{conv}(c^1, \ldots, c^p)$*. That is,*

$$X_{SE}(C) = \{x \in \mathcal{X} \mid D^*(x) \cap \text{int}(\text{conv}(c^1, \ldots, c^p)) \neq \emptyset\}.$$

Proof of Lemma 1. Let $\mathcal{X}$ and $C \in \mathbb{R}^{p \times n}$ be given. First, suppose $x \in X_{SE}(C)$. Then for some $\lambda \in (0, 1)^p$ with unit sum, x is optimal for $\lambda^\top C$. Hence $\lambda^\top C \in D^*(x)$. Because $\lambda^\top C \in \text{int}(\text{conv}(c^1, \ldots, c^p))$, we have the forward subset relation. Second, let $x \in \mathcal{X}$ such that there exists $\bar{C} \in D^*(x) \cap \text{int}(\text{conv}(c^1, \ldots, c^p))$. Since $\bar{C}$ is a convex combination of c^i, there exists at least one vector of convex multipliers $\lambda \in (0, 1)^p$ with unit sum such that $\bar{C} = \lambda^\top C$. Then x is optimal to a weighted sum scalarization, and hence it is a supported efficient solution for C. This concludes the backward subset relation. □

The interior of the convex hull excludes boundary cases that would lead to weakly efficient solutions, which are dominated. Lemma 1 implies some intuitive corollaries. First, if the zero objective vector is a convex combination of objectives, then every solution is supported.

Corollary 1. *If* $0 \in \text{int}(\text{conv}(c^1, \ldots, c^p))$*, then* $X_{SE}(C) = \mathcal{X}$*. If* $x \in \bar{X}_{SE}$ *and* $D^*(x) = \{\vec{0}\}$*, then either* $\bar{X}_{SE} = \mathcal{X}$ *or* $D^*_{SE}(\bar{X}, \bar{X}_{SE}) = \emptyset$*.*

Corollary 1 is naturally limited in scope, especially with respect to binary programs where every feasible solution is an extreme point of $\text{conv}(\mathcal{X})$. Therefore, $D^*(x)$ is nonsingleton for every feasible $x \in \mathcal{X}$, and so Corollary 1 is never applicable. Although, a certificate of infeasibility is useful, since certifying an outer approximation, D^*_{SE}, as infeasible guarantees the inverse-feasible set, D^*_E, is infeasible.

A second corollary relates to the *ideal point*, which is the image defined component-wise as the optimal value for every objective, *i.e.*, $y^I_i := \max\{c^i x \mid x \in \mathcal{X}\}$ for $i = 1, \ldots, p$. When the ideal point is a feasible image, the ND frontier is just the singleton $\{y^I\}$. It is commonplace in multiobjective contexts to assume that the ideal point is infeasible. In our context, a similar case is associated with having a singleton target set, *i.e.*, $|\bar{X}| = 1$. The following claim identifies that this case leads to the multiobjective inverse-feasible set reducing to the single-objective inverse-feasible set.

Corollary 2. *If* $\bar{X} = \bar{X}_{SE} = \{\bar{x}\}$*, then* C *is inverse-feasible if and only if* $c^i \in D^*(\bar{x})$ *for all* $1 \leq i \leq p$*. Equivalently,* $D^*_E(\bar{X}, \bar{X}_{SE}) = D^*(\bar{x}) \times \cdots \times D^*(\bar{x}) = [D^*(\bar{x})]^p$*.*

The hypercube structure can be observed in two dimensions via Figure 2c where the inverse-feasible regions for singleton sets are squares.

Next, we consider more complex cases. We are interested in whether the union of cones $\cup_{x \in \bar{X}_{SE}} D^*(x)$ remains convex or not. Since each individual cone is convex, there are two cases of nonconvexity. First is the case of non-pointed cones, *i.e.*, those that contain a line. (The second case is addressed in the subsequent section.) For example, in Figure 5, $D^*(x^0) \cup D^*(x^1) \cup D^*(x^4)$ is nonconvex. This case is reasonable to address by an assumption, which is motivated by applications where we assume that the target set of supported solutions is possible to achieve. We interpret this to mean that the target supported set coexists on one region of the feasible set's boundary. Assumption 1 geometrically translates this to the inverse vector space.

Assumption 1. *For given* $\bar{X}_{SE}$*, there exists a pointed cone* P *in inverse-vector space such that* $D^*(x) \subset P$ *for all* $x \in \bar{X}_{SE}$*.*

Proposition 1 provides a sufficient condition to prove an objective matrix belongs to this approximation. Omitted proofs for Propositions are included in Supplementary Materials.

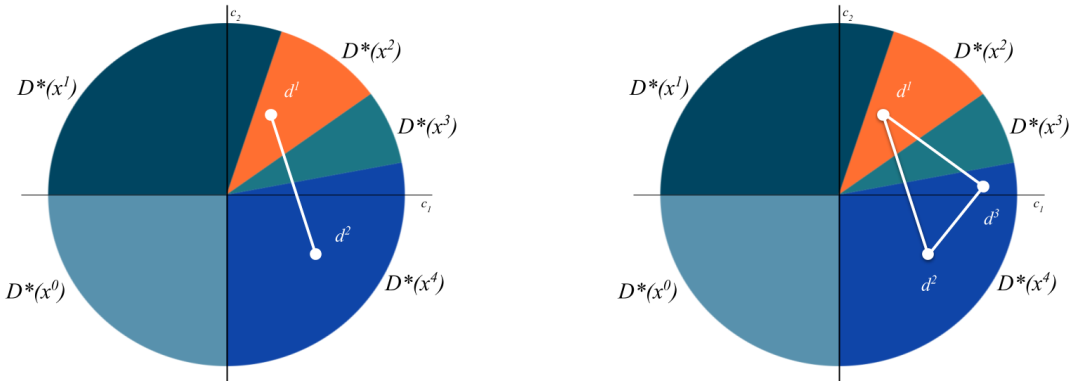

Figure 6: Example 1.5, illustrating Proposition 1.

Proposition 1. *Let $\bar{X}_{SE} \subset \bar{X}_E \subset \mathcal{X}$, $p \geq 2$ be fixed, and $c^1, \ldots, c^p \in \mathbb{R}^n$ be nonzero such that $C := [c^1; \ldots; c^p]$ is not self-collinear. If $D^*(x) \cap \operatorname{int}(\operatorname{conv}(c^1, \ldots, c^p))$ is nonempty for all $x \in \bar{X}_{SE}$ and empty for all $x \notin \bar{X}_{SE}$, then $C \in D^*_{SE}(\bar{X}_{SE})$.*

The following example illustrates Proposition 1.

Example 1.5. *Given $\bar{X}^1 = \{x^2, x^4\}$ and $p = 2$, set $D^*(x^2) \cup D^*(x^4)$ is nonconvex; refer to Figure 1. There does not exist an objective matrix which makes x^2 and x^4 supported without x^3 also being supported. Given $\bar{X}^2 = \{x^2, x^3, x^4\}$, set $D^*(x^2) \cup D^*(x^3) \cup D^*(x^4)$ is convex (Figure 6a). For $p = 2$, matrix $D := [d^1; d^2] \in D^*_{SE}(\bar{X}^2)$. For $p = 3$, we may also choose d^3 so that the convex hull of the vectors intersect only the desired cones (Figure 6b); hence, matrix $D' := [d^1; d^2; d^3] \in D^*_{SE}(\bar{X}^2)$.*

The following are intuitive corollaries of Proposition 1. First is an existence result for the nice case of a convex union of cones.

Corollary 3. *Let $\bar{X}_{SE} \subset \bar{X}_E \subset \bar{X}$, and suppose $\cup_{x \in \bar{X}_{SE}} D^*(x)$ is a pointed, convex cone. Then for some finite $p \geq 2$, $D^*_{SE}(\bar{X}_{SE})$ contains an objective matrix that is not self-collinear.*

For one construction of an inverse-feasible objective matrix, consider intersecting the union of cones with an affine hyperplane to represent normalizing, *e.g.*, $\{c \in \mathbb{R}^n \mid \sum_{i=1}^n c_i = 1\}$. Then extreme points of the resulting polytope

generate an objective matrix feasible to the inverse supported set. By this construction, p is the number of extreme points, which may be quite large.

The second corollary provides that increasing the value of p will maintain feasibility.

Corollary 4. *If $D^*_{SE}(\bar{X}_{SE})$ is nonempty for $\bar{p} \geq 2$, then $D^*_{SE}(\bar{X}_{SE})$ is nonempty for all $p > \bar{p}$.*

Intuitively, since $\bar{p}$ objective vectors construct a sufficiently large convex hull, then choosing additional objective vectors (*e.g.*, within the convex hull) will obviously satisfy the conditions of Proposition 1, as well. Corollary 4 suggests that there is some minimal number of objectives, p^*, for which $D^*(\bar{X}_{SE})$ is nonempty.

5.1. Convex Core

The introduction of *convex cores* permits a more accurate description of D^*_{SE}. For our study, we are interested in the family of pointed cones $\mathcal{F} = \{D^*(x)\}_{x \in \bar{X}_{SE}}$ with a nonconvex union, denoted Π. We would like to inscribe $D^*_{SE}(\bar{X}_{SE})$ as a convex set confined within this nonconvex set. Therefore, as an alternative to the commonplace convex hull (*i.e.*, the smallest convex superset), we are interested in a maximal convex subset contained within.[1] As the following definition details, we additionally require the subset to intersect all component sets of the union.

Definition 5 (Convex core)**.** *Let $\mathcal{F}$ be a family of n-dimensional polyhedra in $\mathbb{R}^n$, and let $\Pi = \cup_{P \in \mathcal{F}} P$ denote their union. Convex set S is a* convex core *of Π if it is a subset of Π which intersects the interior of every $P \in \mathcal{F}$ and is maximal with respect to subset inclusion. That is, there does not exist a convex set $S' \subseteq \Pi$ such that S' intersects every $\text{int}(P)$ and $S \subset S'$. The set of all convex cores is denoted by core(Π).*

See Figure 7 to illustrate a simple family of two-dimensional polyhedra with a nonconvex union and two distinct convex cores. If $\Pi = \cup_{P \in \mathcal{F}} P$ happens to be convex on its own, then it is trivial that it has a *unique* convex core (Π, itself). Unfortunately, in our setting, there is no guarantee

[1] This concept is natural in the context of nonconvex, self-intersecting polytopes. For instance, the convex core of a small stellated dodecahedron is a dodecahedron.

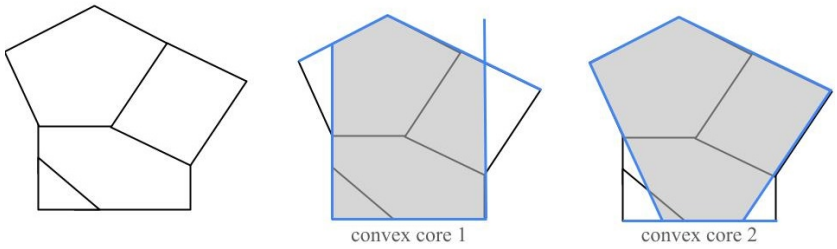

Figure 7: (Left) A family of convex polytopes, $\mathcal{F}$, whose union Π is nonconvex. (Middle) One convex core (in gray) which is representable by a subset of the constraints (in blue). (Right) A second convex core (in gray) which is representable by a subset of the constraints (in blue). Both convex cores have five extreme points and four extreme polyhedra.

that Π has a single, unique convex core. Thus, we more broadly define the *set* of convex cores.

We are unaware of a practical representation or computational method for the convex cores of a general family of polytopes in the literature. For now, we present a rough outline by means of eliminating constraints from the outer descriptions of the polyhedra.

Proposition 2 (Constraint Subset)**.** *For $\mathcal{F} = \{P^1, P^2, \ldots, P^k\}$ and $1 \leq i \leq k$, let $\Pi := \cup_{1 \leq i \leq k} P^i$. Assume each polytope is n-dimensional and has an inequality description in the form of $P^i := \{x \in \mathbb{R}^n \mid A^i x \leq b^i\}$.*

1. *If $Q \in core(\Pi)$ is a convex core of Π, then $Q = \{x \in \mathbb{R}^n \mid A^Q x \leq b^Q\}$ where each constraint from $A^Q x \leq b^Q$ belongs to (at least) one of the systems $A^i x \leq b^i$ for $1 \leq i \leq k$.*
2. *If $a^\top x \leq b$ is a constraint for P^i and $a^\top x \geq b$ is a constraint for P^j where $i \neq j$, then neither constraint are in an outer description for any convex core.*
3. *If $a^\top x \leq b$ is a constraint for P^i and is valid for every polyhedron in the family, then $a^\top x \leq b$ is a valid (possibly redundant) constraint for every convex core of Π.*

In short, Proposition 2 states that every convex core of Π may be represented as a subset of all the constraints used to represent $P^1, \ldots, P^k$.

In the application of inverse MOIP, we have a family of unbounded D^* cones emanating from the origin. It is equivalent but simpler to analyze the family as bounded polytopes, so we introduce a "flattening" affine hyperplane H which can be chosen without loss of generality as long as it has nonempty

intersection with the family of cones. For example, it may be appropriate to choose objectives with unit sum, represented by $H := \{c \in \mathbb{R}^n \mid \sum_{i=1}^n c_i = 1\}$. Once flattened, the extreme points of a convex core are informative, and we link the number of them to the inverse MOIP problem. Consider one convex core for Π. We can offer an interpretation of the extreme points: The set of them guarantees one selection of objective vectors that sufficiently covers the necessary D^* cones. This offers a guarantee of feasibility for that number of objective vectors. One would expect that as the number of extreme points increases, then the number of objective vectors required to cover the necessary D^* cones also increases.

Proposition 3 (Covering Extreme Points)**.** *Let $\mathcal{F}$ represent the family of polyhedra for the intersections of $D^*(x) \cap H$ for every $x \in \bar{X}_{SE}$ and some affine hyperplane H. Denote $\Pi = \cup_{P \in \mathcal{F}} P$. For each convex core $S \in core(\Pi)$, and let κ_S be the number of extreme points of S. Then $D^*_{SE}(\bar{X})$ is nonempty for $p \geq \kappa_S$.*

Determining the minimal number of objectives p^* for nonempty $D^*_{SE}(\bar{X})$ remains an open research question.

5.2. Special Properties for Unit Lattice

In this section, we focus on the following example which is commonly encountered when working with binary decision variables. It is useful for generalizing to higher-dimensions while maintaining a simple structure.

Example 2.0. *Consider for $n \geq 2$ the n-dimensional lattice of unit vectors and the origin, denoted by*

$$\Delta^n := \left\{ x \in \{0,1\}^n \;\middle|\; \sum_{i=1}^n x_i \leq 1,\ x_i \geq 0 \quad \forall i = 1, \ldots, n \right\}.$$

The following facts will be relevant: every $x \in \Delta^n$ is an extreme point of $\mathrm{conv}(\Delta^n)$. Therefore, $D^*(x)$ is a nonsingleton for every $x \in \Delta^n$. The cones may be represented in closed form as

$$D^*(\vec{0}) = \{d \in \mathbb{R}^n \mid d_j \leq 0 \quad \forall j = 1, \ldots, n\} \quad \textit{and}$$

$$D^*(\vec{e_i}) = \{d \in \mathbb{R}^n \mid d_i \geq 0, d_i \geq d_j \quad \forall j \neq i\},$$

where $1 \leq i \leq n$ and $\vec{e}_i$ is the ith unit vector. Furthermore, every pair of feasible solutions of $\mathrm{conv}(\Delta^n)$ are adjacent by an edge. Hence, $D^*(x^1) \cap D^*(x^2)$ is nonempty for every distinct $x^1, x^2 \in \Delta^n$.

Recall that Corollary 4 implies a minimum value of p exists such that $D^*_{SE}(\bar{X}_{SE})$ is nonempty. Specifically for Δ^n, Lemma 2 shows that any subset of the lattice is possible to be supported efficient for even the most restrictive case of $p = 2$. We denote $\{\bar{X}_{SE}, \bar{X}_U\} \subset \Delta^n$ as a nonempty partition of Δ^n, where $\bar{X}_U$ denotes the set of solutions to be either unsupported efficient or non-efficient.

Lemma 2. *Let $\{\bar{X}_{SE}, \bar{X}_U\} \subset \Delta^n$ be a nonempty partition of Δ^n. Then for $p = 2$, $D^*_{SE}(\bar{X}_{SE})$ is nonempty.*

The proof applies the observation that for objective matrix $C \in \mathbb{R}^{p\times n}$, the image set $C\Delta^n$ trivially yields n images equal to the columns of C and additionally the origin. Therefore, any desired image set with n images is attainable by constructing C. We view this simplified optimization problem as an *image selection* problem.

Proof. Let $p \geq 2$, $n \geq 3$, and $\Delta^n = \{x^0, x^1, \ldots, x^n\} \subset \{0, 1\}^n$, where x^0 denotes the origin, and for $1 \leq i \leq n$, x^i denotes the feasible lattice point whose ith coordinate is 1 (remaining coordinates are 0). To simplify this proof, we assume $x^0 \notin \bar{X}_{SE}$, which may be handled with uninteresting modifications. without loss of generality, we assume $\bar{X}_{SE} = \{x^1, \ldots, x^s\}$ for $1 < s \leq n$ (any other solution set follows by permutation). We omit the trivial case where $s = 1$ (see Corollary 2). Recall that both objectives are maximized.

Note that for fixed n, p, s, there exists many frontiers which contain s supported ND images, which may either be constructed randomly or recursively. For such a ND image set, $\tilde{Y}$, let $\{y^1, y^2, \ldots, y^s\}$ be the subset of supported ND images. Use these images to construct the objective coefficients, where all components after the sth are zero, *i.e.*, define

$$c^1 = (y^1_1, y^2_1, \ldots, y^s_1, \vec{0}) \quad \text{and} \quad c^2 = (y^1_2, y^2_2, \ldots, y^s_2, \vec{0})$$

Let $C \coloneqq [c^1; c^2]$. If $x^i \notin \bar{X}_{SE}$ for $1 \leq i \leq n$, then C maps x^i to the origin. Thus we have $C\Delta^n$ has image set $\{y^1, y^2, \ldots, y^s, \vec{0}\}$. Hence, solutions $x^1, \ldots, x^s$ are supported efficient, as desired. □

6. Properties of Inverse Incomparable Set

Whereas supportedness translates directly from single-objective optimization (via weighted sum scalarization), stability is a property unique to multiobjective optimization. Every efficient set is stable, but not vice versa.

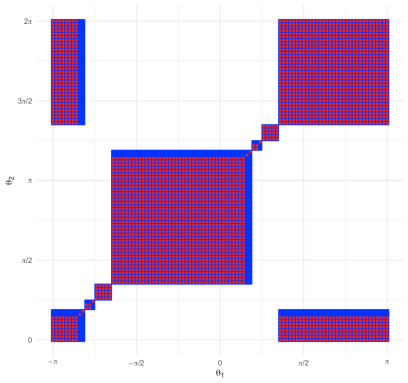

(a) Inverse incomparable sets for $\bar{X}^1$ with 3 solutions (in blue) and $\bar{X}^2$ with 4 solutions (in red).

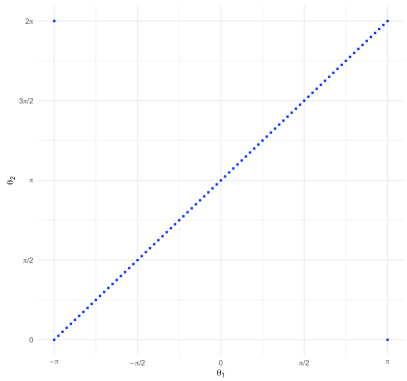

(b) Inverse incomparable sets for $\{x^1, \ldots, x^{100}\}$ uniformly drawn from $x^i \in [0,1] \times [0,1]$.

Figure 8: Inverse incomparable sets ($\tilde{D}$) in θ-space for various solution sets $\bar{X}$. Note that the θ_1-axis has been shifted to the range $[-\pi, +\pi]$ (as opposed to $[0, 2\pi]$ in other figures) to highlight the antiparallel symmetry.

Figure 8 illustrates inverse incomparable sets in θ-space; note that the limits on the θ_1-axis are shifted (compared to other figures) for reasons discussed in Section 6.1.

The first property is that increasing the number of solutions in $\bar{X}$ decreases the region $\tilde{D}(\bar{X})$, which is formalized in Property 5.

Property 5. *If $\bar{X}^1 \subset \bar{X}^2 \subseteq \mathcal{X}$, then $\tilde{D}(\bar{X}^2) \subseteq \tilde{D}(\bar{X}^1)$.*

Example 1.6. *For $\bar{X}^1 = \{x^1, x^2, x^3\}$ and $\bar{X}^2 = \{x^1, x^2, x^3, x^4\}$, $\tilde{D}(\bar{X}^1)$ and $\tilde{D}(\bar{X}^2)$ are shown in Figure 8a, colored blue and red, respectively. Observe that $\tilde{D}(\bar{X}^2) \subseteq \tilde{D}(\bar{X}^1)$, i.e., the inverse incomparable region shrinks when introducing an additional solution.* □

6.1. Anti-Parallel Symmetry

Recall that Property 4 provides that $\tilde{D}(\bar{X})$ is nonempty for any $\bar{X} \subseteq \mathcal{X}$ since all self-collinear objective matrices are elements. By definition of self-collinear, the objective vectors satisfy $c^2 = -\alpha c^1$ for positive α, so the vectors are anti-parallel with π-radians between. Hence, in θ-space, the self-collinear objective matrices appear along the diagonal $\theta_2 = \theta_1 + \pi$ (or $\theta_2 = \theta_1 - \pi$) line. This line can be observed for the running example in Appendix A Figure A.9 for the case of all solutions being efficient. As $\bar{X}$ grows in size, and $\tilde{D}(\bar{X})$ reduces in size to just this diagonal line.

Example 1.7. *Figure 8b shows the inverse incomparable region for 100 points randomly selected from the unit square* $[0,1] \times [0,1]$. *Note that* $\mathcal{X}$ *need not be well-defined here for* $\tilde{D}(\bar{X})$ *to be simulated by brute force. The region* $\tilde{D}(\bar{X})$ *has been reduced to the diagonal line* $\theta_2 = \theta_1 \pm \pi$, *e.g., where the corresponding objective vectors satisfy* $c_1 = -\alpha c_2$ *for some* $\alpha > 0$.

Recall the line of symmetry by permutation, $\theta_2 = \theta_1$, discussed in Section 4.1. The line of self-collinear matrices provides an additional type of symmetry for $\tilde{D}$ which does not appear for D^*_{SE} or D^*_E. Property 6 states this new symmetry, and it may be observed in Figure 8 as the $\theta_2 = \theta \pm \pi$ line appearing in the set $\tilde{D}$ and the $\theta_2 = \theta_1$ line occurring in white space outside of the set. This anti-parallel symmetry may be interpreted as symmetry across the "nearest" self-collinear objective matrix.

Property 6. *Let* $n = p = 2$. *When viewed from* θ*-space,* $\tilde{D}(\bar{X})$ *is symmetric across line* $\theta_2 = \theta_1$ *and across lines* $\theta_2 = \theta_1 \pm \pi$.

6.2. Projection to θ*-space*

For every set $\bar{X} \subseteq \mathcal{X}$, region $\tilde{D}(\bar{X})$ is a union of polyhedral cones in inverse-matrix space emanating from the origin. For $n = p = 2$, this conic structure is amenable to the θ-space representation, wherein a two-dimensional rectangular region in θ-space denotes a cone with four facets in inverse-matrix space. In this biobjective setting, we work with pairs of objective vectors. Property 7 clarifies the structure of the Cartesian product of inverse-feasible regions and its projection to θ-space.

Property 7. *Let* $P^1, P^2 \subset \mathbb{R}^2$ *be pointed cones in inverse-vector space emanating from the origin defined by*

$$P^i \coloneqq \{c \in \mathbb{R}^2 \mid c = (r\cos\theta, r\sin\theta), \quad \alpha_i \leq \theta \leq \beta_i, \quad r \geq 0\}$$

for some $\alpha_1, \alpha_2, \beta_1, \beta_2 \in \mathbb{R}$ *such that* $\alpha_i < \beta_i$ *for* $i = 1, 2$. *Now* $Q \coloneqq P^1 \times P^2 \subset \mathbb{R}^{2\times 2}$ *is a set of matrices in inverse-matrix space. The projection of* Q *to* θ*-space is* $[\alpha_1, \beta_1] \times [\alpha_2, \beta_2] \subset \mathbb{R}^2$, *which is rectangular with sides parallel to both axes and nonempty interior.*

Example 1.8. *In Figure 8a,* $\tilde{D}(\bar{X}^1)$ *is the union of 6 pointed cones, indicated by six blue boxes, where one box continues across the both axes of* θ*-space. Similarly,* $\tilde{D}(\bar{X}^2)$ *is the union of cones strictly contained within* $\tilde{D}(\bar{X}^1)$, *represented by the red boxes.*

Supplementary Materials includes the exhaustive method of computing the precise θ-space representation of $\tilde{D}$, which may offer further intuition.

6.3. Half-Space Covering

Proposition 4 provides a general result for a structural description of $\tilde{D}(\bar{X})$. We use the notation $\text{sign}(A) = -\text{sign}(B)$ to indicate that $A > 0$ and $B < 0$ or vice versa.

Proposition 4. *Let* $\bar{X} = \{x^1, \ldots, x^s\} \subset \mathcal{X} \subset \mathbb{R}^n$ *and* $C = [c^1; \ldots; c^p]$ *for* $c^1, \ldots, c^p \in \mathbb{R}^n$. *Suppose for every distinct pair of solutions* $x^i, x^j \in \bar{X}$ *there exists* $q, r \in \{1, \ldots, p\}$ *such that* $\text{sign}(c^q(x^i - x^j)) = -\text{sign}(c^r(x^i - x^j))$. *Then* $C\bar{X}$ *is stable and* $C \in \tilde{D}(\bar{X})$.

Proof. Assume $n \geq 2, s \geq 2$, and $p \geq 2$. Let $\bar{X}$ and C be as given, and suppose for contradiction that $C\bar{X}$ is not stable. Then there exists $x, x' \in \bar{X}$ such that Cx dominates Cx', *i.e.*, $Cx \geqq Cx'$. So for $i \in \{1, \ldots, p\}$, $c^i x \geq c^i x'$ with at least one inequality strict. Equivalently, $c^i(x - x') \geq 0$ for all $i \in \{1, \ldots, p\}$, which contradicts the assumption that there exists q and r such that $c^q(x - x') > 0$ and $c^r(x - x') < 0$ (or vice versa). □

Supplementary Materials includes many useful examples of Proposition 4 for the reader to build intuition from small values of n, s, and p. In short, Proposition 4 expresses a half-space covering condition which, when satisfied, achieves stability for the target set. Finite n represents the dimension of inverse-vector space (and decision space). The number of solutions, s, determines the number of hyperplanes/half-spaces in the subdivision of the inverse-vector space. Finally, p determines the number of objective vectors to be selected to achieve the covering.

7. Conclusions

This paper presents two outer approximations for D_E^*. Although not an exact representation, we believe together they form a close approximation. We denote the *characterization gap* of this approximation by

$$\Gamma(\bar{X}, \bar{X}_{SE}) \coloneqq D_{SE}^*(\bar{X}_{SE}) \cap \tilde{D}(\bar{X}) - D_E^*(\bar{X}, \bar{X}_{SE}).$$

The gap may be nonempty when $\bar{X}_{SE} \subset \bar{X} \subset \mathcal{X}$ (both subsets strict) and depends on the dominated solutions and unsupported efficient solutions. Supplementary Materials include a proof that the gap is nonempty with an example.

This work has established fundamental structures for inverse optimization of MOIP by extending ideas from single-objective optimization and augmenting with concepts unique to multiobjective optimization. Two outer approximations were developed for the target inverse-feasible set, D_E^*. First, supported images, characterized via single-objective optimization and viewed through the lens of convex combinations, led to the inverse supported set, D_{SE}^*. Second, the multiobjective notion of incomparable solutions led to the inverse incomparable set, $\tilde{D}$. We demonstrated examples of each outer approximation and important structural properties, including convex-adjacent properties, which would be pertinent to computational approaches. Lastly, we describe the known characterization gap between the target set and intersection of two outer approximations. Much remains to be explored in future research for reducing this gap with novel outer approximations, delving into the convex-adjacent properties, and implementing these insights into computational algorithms.

8. Acknowledgments

This research was supported by Office of Naval Research (N00014-21-1-2262). The views expressed in this article are those of the author(s) and do not reflect the official policy or position of the U.S. Naval Academy, Department of the Navy, the Department of Defense, or the U.S. Government.

Appendix A. Inverse-Feasible Regions for Running Example

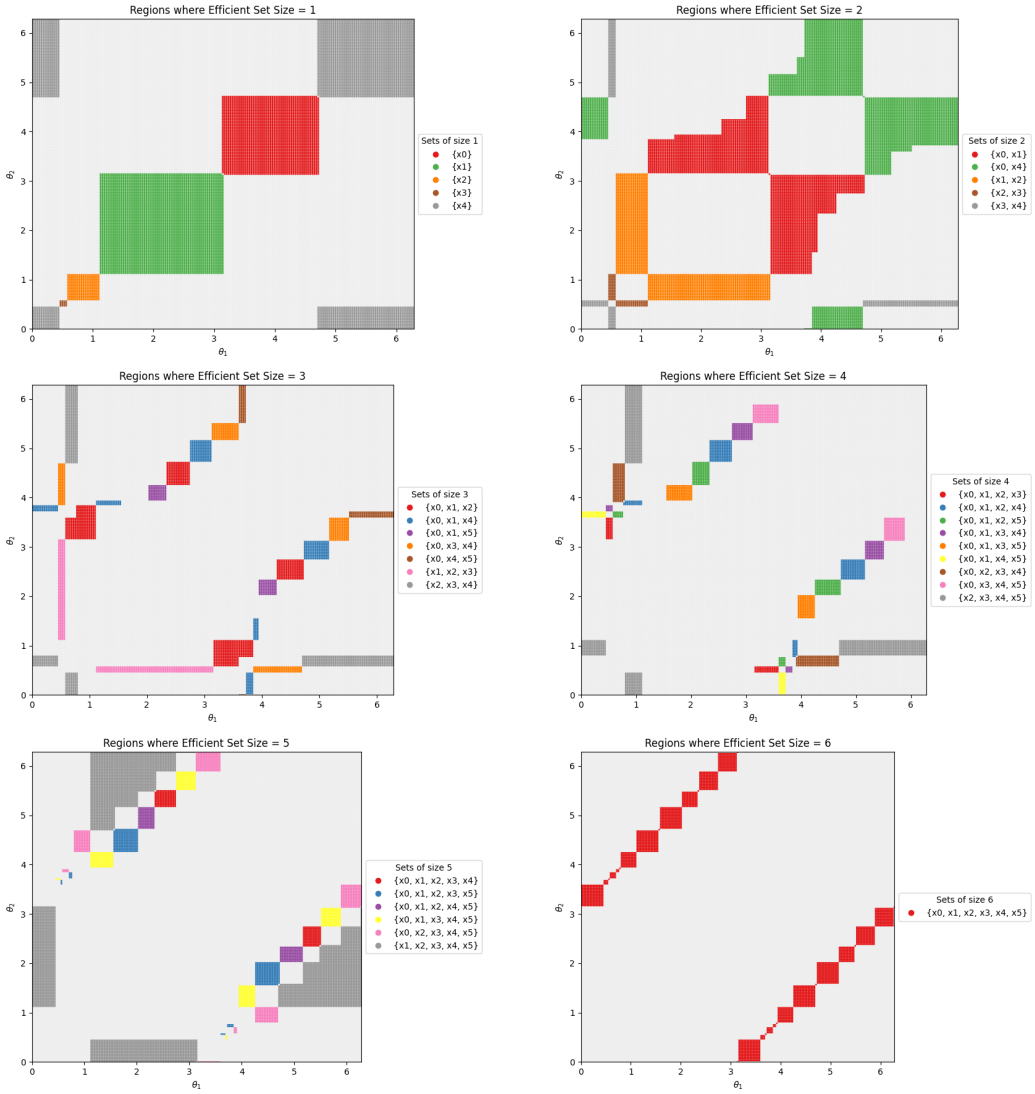

Figure A.9: Inverse-feasible regions for the running example, separated by cardinality of the efficient set.

References

Agarwal, R. and Ergun, Ö. (2008). Mechanism design for a multicommodity flow game in service network alliances. *Operations Research Letters*, 36(5):520–524.

Ahuja, R. K. and Orlin, J. B. (2001). Inverse optimization. *Operations Research*, 49(5):771–783.

Alves, M. J. and Costa, J. P. (2016). Graphical exploration of the weight space in three-objective mixed integer linear programs. *European Journal of Operational Research*, 248(1):72–83.

Andersson, J. (2000). A survey of multiobjective optimization in engineering design. *Department of Mechanical Engineering, Linktjping University. Sweden*, pages 1–34.

Bertsimas, D., Gupta, V., and Paschalidis, I. C. (2015). Data-driven estimation in equilibrium using inverse optimization. *Mathematical Programming*, 153:595–633.

Birge, J. R., Hortaçsu, A., and Pavlin, J. M. (2017). Inverse optimization for the recovery of market structure from market outcomes: An application to the MISO electricity market. *Operations Research*, 65(4):837–855.

Boutilier, J. J., Lee, T., Craig, T., Sharpe, M. B., and Chan, T. C. (2015). Models for predicting objective function weights in prostate cancer IMRT. *Medical Physics*, 42(4):1586–1595.

Burton, D. and Toint, P. L. (1992a). On an instance of the inverse shortest paths problem. *Mathematical Programming*, 53:45–61.

Burton, D. and Toint, P. L. (1992b). On an instance of the inverse shortest paths problem. *Mathematical Programming*, 53:45–61.

Burton, D. and Toint, P. L. (1994). On the use of an inverse shortest paths algorithm for recovering linearly correlated costs. *Mathematical Programming*, 63:1–22.

Carr, S. and Lovejoy, W. (2000). The inverse newsvendor problem: Choosing an optimal demand portfolio for capacitated resources. *Management Science*, 46(7):912–927.

Chakraborty, S., Raut, R. D., Rofin, T., and Chakraborty, S. (2023). A comprehensive and systematic review of multi-criteria decision-making methods and applications in healthcare. *Healthcare Analytics*, page 100232.

Chan, T. C., Craig, T., Lee, T., and Sharpe, M. B. (2014). Generalized inverse multiobjective optimization with application to cancer therapy. *Operations Research*, 62(3):680–695.

Chan, T. C. and Kaw, N. (2020). Inverse optimization for the recovery of constraint parameters. *European Journal of Operational Research*, 282(2):415–427.

Chan, T. C., Mahmood, R., and Zhu, I. Y. (2023). Inverse optimization: Theory and applications. *Operations Research*.

Dial, R. B. (1999). Minimal-revenue congestion pricing part I: A fast algorithm for the single-origin case. *Transportation Research Part B: Methodological*, 33(3):189–202.

Duan, Z. and Wang, L. (2011). Heuristic algorithms for the inverse mixed integer linear programming problem. *Journal of Global Optimization*, 51:463–471.

Dunbar, A., Sinha, S., and Schaefer, A. J. (2024). Relaxations and duality for multiobjective integer programming. *Mathematical Programming*, 207(1):577–616.

Ehrgott, M. (2005). *Multicriteria Optimization*. Springer Science & Business Media.

Ehrgott, M. and Gandibleux, X. (2002). Multiobjective combinatorial optimization—theory, methodology, and applications. *Multiple Criteria Optimization: State of the Art Annotated Bibliographic Surveys*, pages 369–444.

Ehrgott, M., Güler, Ç., Hamacher, H. W., and Shao, L. (2010). Mathematical optimization in intensity modulated radiation therapy. *Annals of Operations Research*, 175(1):309–365.

Emelichev, V. and Podkopaev, D. (2010). Quantitative stability analysis for vector problems of 0–1 programming. *Discrete Optimization*, 7(1-2):48–63.

Erkin, Z., Bailey, M. D., Maillart, L. M., Schaefer, A. J., and Roberts, M. S. (2010). Eliciting patients' revealed preferences: An inverse Markov decision process approach. *Decision Analysis*, 7(4):358–365.

Ghatrani, Z. and Ghate, A. (2023). Inverse Markov decision processes with unknown transition probabilities. *IISE Transactions*, 55(6):588–601.

Ghobadi, K. and Mahmoudzadeh, H. (2021). Inferring linear feasible regions using inverse optimization. *European Journal of Operational Research*, 290(3):829–843.

Hamacher, H. W. and Küfer, K.-H. (2002). Inverse radiation therapy planning—a multiple objective optimization approach. *Discrete Applied Mathematics*, 118(1-2):145–161.

Helfrich, S., Perini, T., Halffmann, P., Boland, N., and Ruzika, S. (2023). Analysis of the weighted Tchebycheff weight set decomposition for multi-objective discrete optimization problems. *Journal of Global Optimization*, 86(2):417–440.

Heuberger, C. (2004). Inverse combinatorial optimization: A survey on problems, methods, and results. *Journal of Combinatorial Optimization*, 8(3):329–361.

Houghtalen, L., Ergun, Ö., and Sokol, J. (2011). Designing mechanisms for the management of carrier alliances. *Transportation Science*, 45(4):465–482.

Iyengar, G. and Kang, W. (2005). Inverse conic programming with applications. *Operations Research Letters*, 33(3):319–330.

Keshavarz, A., Wang, Y., and Boyd, S. (2011). Imputing a convex objective function. In *2011 IEEE international symposium on intelligent control*, pages 613–619. IEEE.

Köksalan, M. and Karakaya, G. (2021). Evaluating solutions and solution sets under multiple objectives. *European Journal of Operational Research*, page 16–28.

Lamperski, J. B. and Schaefer, A. J. (2015). A polyhedral characterization of the inverse-feasible region of a mixed-integer program. *Operations Research Letters*, 43(6):575–578.

Lee, T., Hammad, M., Chan, T. C., Craig, T., and Sharpe, M. B. (2013). Predicting objective function weights from patient anatomy in prostate IMRT treatment planning. *Medical Physics*, 40(12):121706.

Marcotte, P., Mercier, A., Savard, G., and Verter, V. (2009). Toll policies for mitigating hazardous materials transport risk. *Transportation Science*, 43(2):228–243.

Marler, R. T. and Arora, J. S. (2004). Survey of multi-objective optimization methods for engineering. *Structural and Multidisciplinary Optimization*, 26:369–395.

Naghavi, M., Foroughi, A. A., and Zarepisheh, M. (2019). Inverse optimization for multi-objective linear programming. *Optimization Letters*, 13(2):281–294.

Neumann-Denzau, G. and Behrens, J. (1984). Inversion of seismic data using tomographical reconstruction techniques for investigations of laterally inhomogeneous media. *Geophysical Journal International*, 79(1):305–315.

Przybylski, A., Gandibleux, X., and Ehrgott, M. (2010). A recursive algorithm for finding all nondominated extreme points in the outcome set of a multiobjective integer programme. *INFORMS Journal on Computing*, 22(3):371–386.

Roland, J., De Smet, Y., and Figueira, J. R. (2013). Inverse multi-objective combinatorial optimization. *Discrete Applied Mathematics*, 161(16-17):2764–2771.

Roland, J., Figueira, J. R., and De Smet, Y. (2016). Finding compromise solutions in project portfolio selection with multiple experts by inverse optimization. *Computers & Operations Research*, 66:12–19.

Roland, J., Smet, Y. D., and Figueira, J. R. (2012). On the calculation of stability radius for multi-objective combinatorial optimization problems by inverse optimization. *4OR*, 10(4):379–389.

Ruiz, C., Conejo, A. J., and Bertsimas, D. J. (2013). Revealing rival marginal offer prices via inverse optimization. *IEEE Transactions on Power Systems*, 28(3):3056–3064.

Schaefer, A. J. (2009). Inverse integer programming. *Optimization Letters*, 3(4):483–489.

Tarantola, A. (2005). *Inverse Problem Theory and Methods for Model Parameter Estimation*. SIAM.

Tavaslıoğlu, O., Lee, T., Valeva, S., and Schaefer, A. J. (2018). On the structure of the inverse-feasible region of a linear program. *Operations Research Letters*, 46(1):147–152.

Troutt, M. D., Pang, W.-K., and Hou, S.-H. (2006). Behavioral estimation of mathematical programming objective function coefficients. *Management Science*, 52(3):422–434.

Wang, L. (2009). Cutting plane algorithms for the inverse mixed integer linear programming problem. *Operations Research Letters*, 37(2):114–116.

White, D. (1990). A bibliography on the applications of mathematical programming multiple-objective methods. *Journal of the Operational Research Society*, 41(8):669–691.

Zhang, J., Pourazarm, S., Cassandras, C. G., and Paschalidis, I. C. (2016). The price of anarchy in transportation networks by estimating user cost functions from actual traffic data. In *2016 IEEE 55th Conference on Decision and Control (CDC)*, pages 789–794. IEEE.

Zhang, J., Pourazarm, S., Cassandras, C. G., and Paschalidis, I. C. (2018). The price of anarchy in transportation networks: Data-driven evaluation and reduction strategies. *Proceedings of the IEEE*, 106(4):538–553.

Zhang, J. and Xu, C. (2010). Inverse optimization for linearly constrained convex separable programming problems. *European Journal of Operational Research*, 200(3):671–679.

Zhang, J. and Zhang, L. (2010). An augmented Lagrangian method for a class of inverse quadratic programming problems. *Applied Mathematics and Optimization*, 61(1):57.

Zheng, J., Gao, Z., Yang, D., and Sun, Z. (2015). Network design and capacity exchange for liner alliances with fixed and variable container demands. *Transportation Science*, 49(4):886–899.